Volume 1 | Number 1 | Jan 2013 | Pages 1–100

Journal of
Materials Chemistry A

Materials for energy and sustainability
www.rsc.org/materialsA

Li⁺

ROYAL SOCIETY
OF CHEMISTRY

ROYAL SOCIETY
OF CHEMISTRY

www.rsc.org/materialsA

High-performance $SrNb_{0.1}Co_{0.9-x}Fe_xO_{3-\delta}$ perovskite cathodes for low temperature solid oxide fuel cells

Yinlong Zhu,[a] Jaka Sunarso,[b] Wei Zhou,*[c] Shanshan Jiang [a] and Zongping Shao*[d]

Chemical to electrical energy conversion using solid oxide fuel cell (SOFC) becomes more practical as the operating temperature is lowered to 600 °C and below. Given the thermally activated nature of the oxygen reduction reaction
10 **(ORR) at the cathode side, development of cathode catalyst with very low polarisation resistance is essential. Here, we showed that partial substitution of Co within $SrNb_{0.1}Co_{0.9}O_{3-\delta}$ by Fe (up to 0.5) triggers the formation of oxygen non-stoichiometry while preserving the primitive cubic lattice,**
15 **thus substantially enhancing the ORR performance below 600 °C (relative to the parent compound). Close correlation between the oxygen non-stoichiometry and ORR activity trends was implied to some extent. $SrNb_{0.1}Co_{0.7}Fe_{0.2}O_{3-\delta}$ (SNFC0.2) cathode exhibits a very low area specific resistance**
20 **value of 0.052 Ω cm² at 600 °C which translates to superior fuel cell performance e.g. peak power density of 1587 mW cm⁻² at 600 °C. Moreover, the synergistic relationship between ORR activity, thermal expansion coefficient and enhanced CO₂ resistance warrants SNFC cathode significance. The last**
25 **attribute is envisioned as a dominant factor for applications using alternative fuels (e.g. CO which normally contains CO₂) and in a portable single chamber SOFC.**

1. Introduction

30 Of all available technologies to convert chemical-based energy resources to electricity, fuel cell is the most attractive one in terms of conversion efficiency (it can overcome the combustion limitation e.g. Carnot cycle) and fuel flexibility. This is particularly true for solid oxide fuel cells (SOFCs). In this device,
35 O_2 reacts with electron (in the cathode), to produce oxygen ions which are then transported (through the electrolyte), and react with fuel (in the anode) to produce electrons at a distinct potential (from the electron at the cathode side).[1, 2] The use of oxygen ionic conductors as an electrolyte allows other than H_2 fuels such as
40 hydrocarbon and CO.[3] Low temperature SOFC (LT-SOFC) concept (with operating temperature of 400-600 °C) has currently been brought forward to surpass (SOFC's) current economic and technical barriers such as high system costs and degradation pace in conjunction with slow start-up and shut-down cycle.[4] At these
45 temperatures nonetheless, cathode kinetics becomes a major limiting step to obtain good performance.[5,6]

The effective oxygen reduction reaction (ORR) area in the cathode can be enlarged by adopting mixed ionic-electronic conducting (MIEC) perovskites instead of conventional electronic
50 conductor perovskites (e.g. $La_{1-x}Sr_xMnO_3$); therefore bringing down the operating temperature (for conventional SOFC) of 800-1000 °C to 650-800 °C, the latter of which is known as intermediate temperature SOFCs.[7-13] $SrCoO_{3-\delta}$ (SC)-based perovskites exemplifies a MIEC cathode benchmark, made well-
55 known, when in 2004, Shao and Haile demonstrated working SOFC device utilising $Ba_{0.5}Sr_{0.5}Co_{0.8}Fe_{0.2}O_{3-\delta}$ (BSCF) cathode with peak power density of ~1000 mW cm⁻² at 600 °C.[10] Later on, a comparable performance was also reported using $SrSc_{0.2}Co_{0.8}O_{3-\delta}$ (SSC) and $SrNb_{0.1}Co_{0.9}O_{3-\delta}$ (SNC) cathodes.[14,15]

60 If their susceptibility to CO_2 and high thermal expansion coefficients (TEC) can be addressed, it would be practical to incorporate these SC-based cathodes to realise LT-SOFC.[16-18] CO_2 resistance would specially be crucial for application in single-chamber SOFC.[7,19,20]

65 Here we report new cathodes within a perovskite framework of $SrNb_{0.1}Co_{0.9-x}Fe_xO_{3-\delta}$ (SNCF, 0.1≤x≤0.5). These cathodes show excellent ORR activity at low temperatures and more importantly, low TEC values and CO_2 resistance. SNCF0.2, for example shows the lowest area specific resistance value (which is
70 inversely proportional to the ORR activity) of only 0.301 and 0.111 Ω cm² at 500 and 550 °C, respectively. Of significant interest is the moderate thermal activation energy (E_a) value for ASRs of SNCF0.2 (i.e. 94 kJ mol⁻¹), since high activation energy value implies rapid performance deterioration with decreasing
75 temperature. Accordingly, high peak power densities of 610 and 1587 mW cm⁻² were achieved on an anode-supported 20 μm $Sm_{0.2}Ce_{0.8}O_{1.9}$ (SDC) single fuel cell at 500 and 600 °C.

2. Experimental Section

80 *Synthesis of powders:* $SrNb_{0.1}Co_{0.9-x}Fe_xO_{3-\delta}$(x=0, 0.1, 0.2, 0.3 and 0.5) powders were synthesised using a solid-state reaction route. Stoichiometric amounts of $SrCO_3$, Nb_2O_5, Co_2O_3 and Fe_2O_3 (all analytical grade, Sinopharm Chemical Reagent Co. Ltd.) were weighed, mixed and milled in a planetary mill
85 (Fritsch, Pulverisette 6) using acetone as a solvent media at 400 rpm for 1 h. After drying, the powders mixture was calcined at 1200 °C in air for 10 h. The milling and calcination were repeated again to obtain single phase $SrNb_{0.1}Co_{0.9-x}Fe_xO_{3-\delta}$.

Fabrication of the symmetrical cells and the single fuel cell:
90 Symmetrical cells with electrode|SDC|electrode configuration were fabricated for electrochemical impedance spectroscopy (EIS) measurements. Dense SDC pellets (0.5 g) of 12 mm in diameter and 0.8 mm thickness were prepared by dry pressing followed by sintering at 1400 °C for 5 h. The cathode powders
95 were first dispersed in a pre-mixed solution of glycerol, ethylene glycol, and isopropyl alcohol. A colloidal suspension was obtained by a planetary milling (Fritsch, Pulverisette 6) at 400 rpm for 0.5 h. The suspension was then deposited symmetrically onto opposing sides of the dense SDC disks using spray
100 deposition. The disk and deposited layers were then calcined at 1000 °C for 2 h in an air atmosphere. The silver paste was then deposited as the current collector.

Anode-supported thin-film electrolyte dual-layer cells were prepared via dual dry-pressing and high-temperature sintering.
105 Anode powders consisting of 60 wt% NiO and 40 wt% SDC were prepared by mixing and milling NiO and SDC powders using an agate mortar and pestle. The green bi-layer electrolyte disks were densified by firing at 1400 °C for 5 h in an air atmosphere. The cathode slurry was then painted onto the whole circular area of
110 the densified electrolyte surface and fired at 1000 °C for 2 h in an air atmosphere. The resultant coin-shaped cathode had an effective area of 0.48 cm².

Basic characterization: The crystal structures were determined by powder X-ray diffraction (D8 Advance, Bruker, Germany) with filtered Cu-Kα radiation (40 kV and 40 mA) using a receiving slit of approximately 0.2–0.4 mm. The diffraction patterns were collected by step scanning between 2θ = 10–90° with a step size of 0.05°. Rietveld refinements of the powder XRD patterns were performed using DIFFRACplus Topas 4.2 software.[21] During the refinements, general parameters, such as the scale factor, background parameters, and the zero point of the counter, were optimised. To simplify the complexity associated with refining large amount of parameters simultaneously, Le Bail refinement was initially used to determine the space group and lattice parameters of the $SrNb_{0.1}Co_{0.9-x}Fe_xO_{3-\delta}$ phases. Rietveld refinement was then used to determine the position of each atom in the lattice.

The oxygen non-stoichiometry and the average of valence states of B-site cation (Co and Fe) at room temperature were determined by iodometric titration. Briefly, approximately 0.1 g of powder was dissolved in a 6 mol^{-1} HCl solution under the protection of a nitrogen atmosphere to prevent the oxidation of I$^-$ ions (from KI) by air, followed by titration with a standard thiosulfate ($S_2O_3^{2-}$) solution. The oxygen non-stoichiometry and the average of valence states of Co and Fe at high temperatures were measured by thermogravimetric analysis (TGA, Model STA 449 F3, NETZSCH) under synthetic air from room temperature to 1000 °C. The heating and cooling rates were 10 °C min^{-1}. Moreover, the oxygen non-stoichiometry (δ) at different temperatures was calculated based on the thermogravimetric data. The oxygen non-stoichiometry at different temperatures in the sample was obtained with the following equation:

$$\delta = \frac{M \times m_o - (M - 15.9994 \times \delta_o) \times m}{15.9994 \times m_o}$$

Where m_o and m are the original weight and the actual weight after heating of the sample, respectively; M is the molar mass of the stoichiometric form of $SrNb_{0.1}Co_{0.9-x}Fe_xO_3$ (0≤x≤0.5); δ_o is the oxygen non-stoichiometry of the sample at the room temperature.

The oxygen desorption properties of the composite powders were probed using oxygen temperature programmed desorption (O$_2$-TPD). For a typical O$_2$-TPD measurement, approximately 0.15 g oxide powders (in the size of 40–60 meshes) were loaded in a U-type quartz tube. Pure argon at a flow rate of 15 ml min^{-1} [STP] (standard temperature and pressure) was fed to the reactor as the carrier gas and the temperature was increased from room temperature to 930 °C at a rate of 10 °C min^{-1}. The effluent gases were analysed by a mass spectrometer (MS, Hiden, QIC-20) to monitor the oxygen concentration.

A bar with the dimensions of 2 mm × 5 mm × 20 mm was sintered at 1100 °C in air to determine the TECs. TECs were measured using a Netsch DIL 402C/3/G dilatometer from 25 °C to 1000 °C with an air-purge flow rate of 50 ml min^{-1}.

The morphologies of the cathode and cathode/electrolyte interface were obtained using an environmental scanning electron microscope (ESEM, QUANTA-2000).

Electrochemical measurements: Electrochemical impedance spectra (EIS) of the cathode was obtained by AC impedance measurements using an electrochemical workstation composed of a Solartron 1260A frequency response analyser and a Solartron 1287 potentiostat. The symmetrical cells were tested between 450–750 °C in an ambient air atmosphere. The applied frequency range was from 0.01 Hz to 100 kHz, and the signal amplitude was 10 mV. The measurement was performed under an open circuit voltage (OCV) condition. Electrode polarisation resistance data were analysed with Z-plot 3.0c software.

The I–V and I–P polarisation curves were collected using a Keithley 2420 source meter based on the four-probe configuration. The single cell test was conducted over an in-lab constructed fuel cell test station within the temperature range of 400-600 °C. During the test, H$_2$ was fed into the anode side as a fuel at a flow rate of 80 ml min^{-1} [STP], while the cathode side was exposed to ambient air.

3. Results and discussion

Fig. 1a depicts room-temperature powder x-ray diffraction (XRD) patterns of $SrNb_{0.1}Co_{0.9-x}Fe_xO_{3-\delta}$ (0≤x≤0.5) perovskites. All compositions exhibit primitive cubic structure with Pm-3m symmetry (space group #221) as confirmed by Rietveld refinement; the lattice parameters of which are listed in **Table 1**. **Fig. 1b** shows magnified section around the most intense peak (e.g. ~32.7°) which shifts gradually to the lower angle for higher Fe content; indicating lattice expansion. This can be rationalised in terms of smaller Co ions (ionic radius of 0.61 Å (Co^{3+}) or 0.53 Å (Co^{4+})) substitution by larger Fe ions (ionic radius of 0.645 Å (Fe^{3+}) or 0.585 Å (Fe^{4+})) ions) (Note: all in high spin at 6-fold coordination).[22, 23]
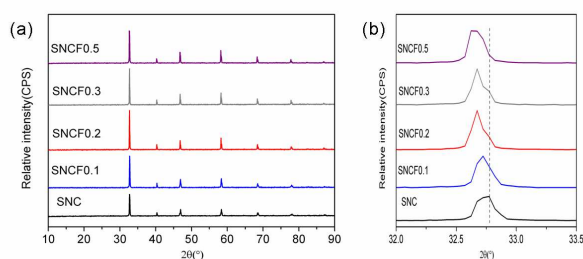

Fig. 1 (a) Powder XRD patterns of SNCF powders calcined at 1200 °C in air for 10 h; (b) Magnified section of powder XRD patterns, 2θ = 32-33.5°.

Oxygen non-stoichiometry (δ) and average valence state (n) of B-site cation (Co and Fe) in SNCF perovskites were obtained using iodometric titration. The results are summarised in **Table 2**. As a general trend, substituting Fe for Co in $SrNb_{0.1}Co_{0.9}O_{3-\delta}$ increases the oxygen non-stoichiometry. The increase is more pronounced for lower amount of Fe dopant. The largest non-stoichiometry was attained when 0.2 Co is substituted by Fe e.g. SNCF0.2. The thermal evolution

Table 1 Lattice parameters of SNCF from Rietveld refinements using Pm-3m space group.

	SNC		SNCF0.1		SNCF0.2		SNCF0.3		SNCF0.5
a	3.8731928	a	3.8782108	a	3.8812964	a	3.8847875	a	3.8866470
Reliability(%)									
Rp	3.11	Rp	3.45	Rp	4.20	Rp	4.50	Rp	4.19
Rwp	4.44	Rwp	4.55	Rwp	5.53	Rwp	6.19	Rwp	6.15
χ^2	1.48	χ^2	1.30	χ^2	1.49	χ^2	1.59	χ^2	1.52

of the oxygen non-stoichiometry and average valence state of B-site cation was probed using thermal gravimetric analysis in air; the results of which are shown as **Fig. 2**. All compositions shows analogous trend of increase of δ and decrease of n. As such, the initial values at room temperature become the determining factor. It is worthwhile to note that the average valence states of Co and Fe approaches 3+ between 500 and 600 ^{o}C. In the absence of interaction between oxygen vacancies and ordering phenomena and when electronic conductivity is not a limiting factor, ORR activity normally correlates with the oxygen non-stoichiometry.[14,15,24-27] This can be understood considering the oxygen vacancies role as the oxygen ions diffusion pathway within the bulk material, effectively extending the ORR from the cathode⎮electrolyte⎮oxygen three phase boundaries (TPB) to the whole cathode surface. Higher oxygen diffusion rate therefore translates to larger cathode surface for ORR. In short, the oxygen vacancies supply the active sites for oxygen adsorption (e.g. oxygen dissociation) at cathode surface.[5]

Table 2 Oxygen non-stoichiometry (δ) and average valence states of B-site (n) of SNCF at room temperature.

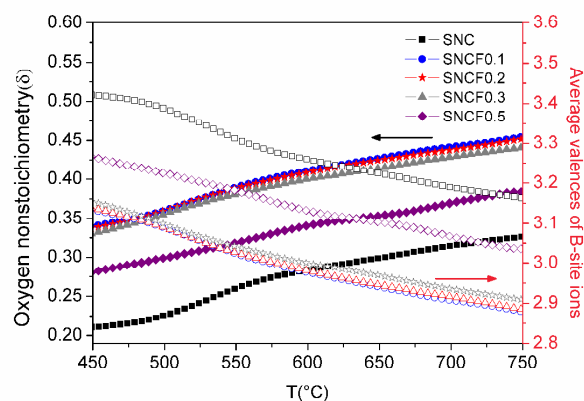| Sample	δ	n
SNC	0.23	3.4
SNCF0.1	0.33	3.2
SNCF0.2	0.34	3.1
SNCF0.3	0.31	3.2
SNCF0.5	0.25	3.3

Fig. 2 The oxygen nonstoichiometry (δ) and average valence states of B-site cation (n) between 450-750 ^{o}C.

The ORR activity of the SNCF (0≤x≤0.5) cathodes was quantified by electrochemical impedance spectroscopy using symmetric cells with $Sm_{0.2}Ce_{0.8}O_{1.9}$ (SDC) as an electrolyte. **Fig. 3a** shows the resultant Nyquist plots between
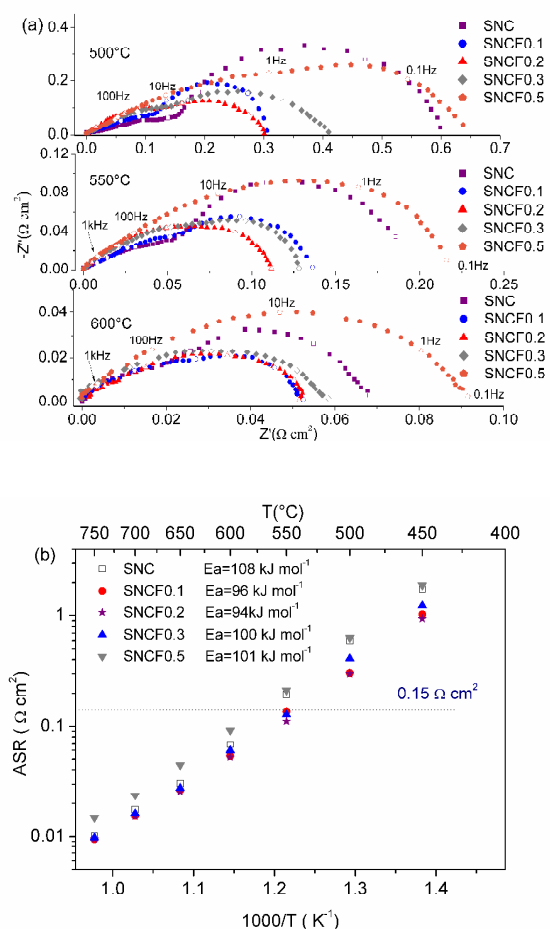

Fig. 3 (a) Electrochemical impedance spectra of SNCF cathodes at 500 °C, 550 °C and 600 °C; (b) Arrhenius plot of ASRs for SNCF cathodes between 450 and 750 °C.

500 and 600 ^{o}C. The area specific resistance (ASR) of the cathode is obtained from the difference between the low frequency and the high-frequency intercepts on the real axis and represents the resistance of the cathode. Except for SNCF0.5, all doped compositions provide lower ASR values (relative to SNC). Quite significant here is the fact that the resistances of the three doped compositions, SNCF0.1, SNCF0.2 and SNCF0.3 at 550 ^{o}C were below a target ASR value of 0.15 Ω cm^2 (below 550 ^{o}C) specified by Steele et al.[28] We note that the best composition, SNCF0.2 delivered the lowest ASR values of 0.301, 0.111 and 0.052 Ω cm^2 at 500, 550 and 600 ^{o}C, respectively. As a comparison, SNC cathode prepared at identical condition showed ASR values of 0.600, 0.195 and 0.068 Ω cm^2 at 500, 550 and 600 ^{o}C, respectively; approximately 30-100% higher. Notably, at 450 ^{o}C (the lowest measured temperature), a relatively low ASR 0.937 Ω cm^2 was attained for SNFC0.2; much favorable compared to 1.74 Ω cm^2 for SNC. These observations together with the thermal activation energy (E_a) for ASRs of SNCF (0.1≤x≤0.5) cathodes are evident in **Fig. 3b**. While SNC cathode exhibited E_a value of 108 kJ mol^{-1}, SNCF0.2 provided a lower value of 94 kJ mol^{-1} which is deemed more favorable to retain high performance at lower temperatures. The mapping of performance of SNFC0.2 against other high performance

perovskite cathodes in the form of Arrhenius plots is shown in **Fig. S1**. This figure include Co-based cathodes represented by $La_{0.6}Sr_{0.4}CoO_{3-\delta}$,[29] $SrSc_{0.2}Co_{0.8}O_{3-\delta}$,[15] $SrNb_{0.1}Co_{0.9}O_{3-\delta}$,[14] $SrSc_{0.175}Nb_{0.025}Co_{0.8}O_{3-\delta}$,[30] layered structure materials such as
5 $PrBaCo_2O_{5+\delta}$,[31] $Sr_{0.95}Nb_{0.1}Co_{0.9}O_{3-\delta}$,[32] and double perovskite, $Ba_2Bi_{0.1}Sc_{0.2}Co_{1.7}O_{6-\delta}$.[26] Several Fe doped Co-based cathodes are also incorporated, for example $Ba_{0.5}Sr_{0.5}Co_{0.8}Fe_{0.2}O_{3-\delta}$ (BSCF), [10] $La_{0.6}Sr_{0.4}Co_{0.2}Fe_{0.8}O_{3-\delta}$,[33] $La_{0.3}Ba_{0.7}Co_{0.6}Fe_{0.4}O_{3-\delta}$,[34] $BaCo_{0.7}Fe_{0.2}Nb_{0.1}O_{3-\delta}$,[35] and layered structure materials such
10 as $PrBa_{0.5}Sr_{0.5}Co_{1.5}Fe_{0.5}O_{5+\delta}$,[36] $GdBa_{0.5}Sr_{0.5}Co_{1.0}Fe_{1.0}O_{5+\delta}$,[37] and $NdBaCo_{1.5}Fe_{0.5}O_{5+\delta}$.[38] SNCF0.2 cathode shows the lowest ASR and E_a values among all the listed cathodes which highlights its potential towards enabling low temperature SOFCs.

15

Table 3 Fitted impedance spectra values for SNCF (0≤x≤0.5) cathodes between 550 and 650 °C.

Sample	Resistances (Ω cm^2)					
	550 °C		600 °C		650 °C	
	R_{E1}	R_{E2}	R_{E1}	R_{E2}	R_{E1}	R_{E2}
SNC	0.060	0.135	0.025	0.043	0.014	0.016
SNCF0.1	0.065	0.071	0.035	0.018	0.017	0.009
SNCF0.2	0.072	0.039	0.036	0.016	0.018	0.007
SNCF0.3	0.092	0.036	0.045	0.014	0.019	0.009
SNCF0.5	0.120	0.091	0.053	0.040	0.030	0.014

More information can be obtained from the impedance
20 spectra (Fig. 3a) to evaluate the ORR kinetics of SNCF cathodes. Therefore, equivalent circuit model containing the series resistor and parallel resistor/constant phase element components with a configuration of R_{Ω}-(R_{E1}-CPE_1)-(R_{E2}-CPE_2) were used to fit the spectra. Our previous studies
25 demonstrate the suitability of this model for mixed ionic-electronic conducting cathodes having high oxygen vacancy concentration such as $Ba_{0.5}Sr_{0.5}Co_{0.8}Fe_{0.2}O_{3-\delta}$ (BSCF), $SrSc_{0.2}Co_{0.8}O_{3-\delta}$, $SrNb_{0.1}Co_{0.9}O_{3-\delta}$ and $SrNb_{0.1}Fe_{0.9}O_{3-\delta}$ cathodes.[14,15,39,40] In this model, R_{Ω} is the ohmic resistance
30 from the electrolyte, electrode and lead; CPE_1 and CPE_2 are constant phase elements. Resistance at high frequency represents the resistance of the charge transfer processes (R_{E1})

which include the electron-transfer and ion transfer processes, occurring at the current collector/electrode and the
35 electrode/electrolyte interfaces, respectively. Resistance at low frequency, on the other hand, represents the resistance of non-charge-transfer processes (R_{E2}) which include adsorption of oxygen, oxygen diffusion at the gas-cathode surface interface and surface diffusion of intermediate oxygen
40 species.[41-43] The deconvoluted results are listed in **Table 3**. For SNC, R_{E2} values are larger than R_{E1} values, indicating relatively slow non-charge transfer processes on SNC cathode surface (compared to charge transfer processes). Partial substitution of Co with Fe creates additional oxygen vacancies
45 which enhances non-charge transfer processes as evidenced by lowering R_{E2} values. The oxygen vacancies trend somewhat correlates with R_{E2} values in the order of SNFC0.1-0.3 followed by SNFC0.5. Recently, Kuklja et al.[44] employed combined theoretical and experimental analysis to evaluate
50 the relationship between surface oxygen vacancy and ORR and analyse the rate-determining step on ORR mechanism of $(La,Sr)MnO_3$, $(La,Sr)(Co,Fe)O_3$ and $(Ba,Sr)(Co,Fe)O_3$ cathodes. Such study is beyond the scope of this work however the trend observed here is quite consistent with the
55 work of Kulkja et al. which highlights the role of enhanced oxygen vacancy concentration to promote oxygen surface exchange processes.[10,44,45] It is worth noting that a lower ORR activity was obtained for SNCF0.5 relative to SNC although the oxygen vacancy concentration is higher for SNCF0.5.
60 Increasing Fe doping consistently leads to increased R_{E1} values which reach their maximum values at 50% Fe, the highest doping amount tested in this work. Upon comparing R_{E1} and R_{E2} values for SNFC0.5 (**Table 3**), the contribution from R_{E1} (charge transfer processes) clearly outweighs that
65 from R_{E2} (non-charge transfer processes) and becomes the limiting factor. This can simply be understood from the higher content of less redox active Fe (relative to Co)[29,31,46,47] which is likely to impede the charge transfer processes. Another piece of supporting evidence can be found in our previous
70 work[40] which reports an analogous perovskite compound where Co is completely replaced with Fe e.g. $SrNb_{0.1}Fe_{0.9}O_{3-\delta}$ (SNF). R_{E1} values for SNF are 0.6, 0.3 and 0.15 Ω cm^2 at 550, 600 and 650 °C which are substantially higher than those for SNCF0.5.
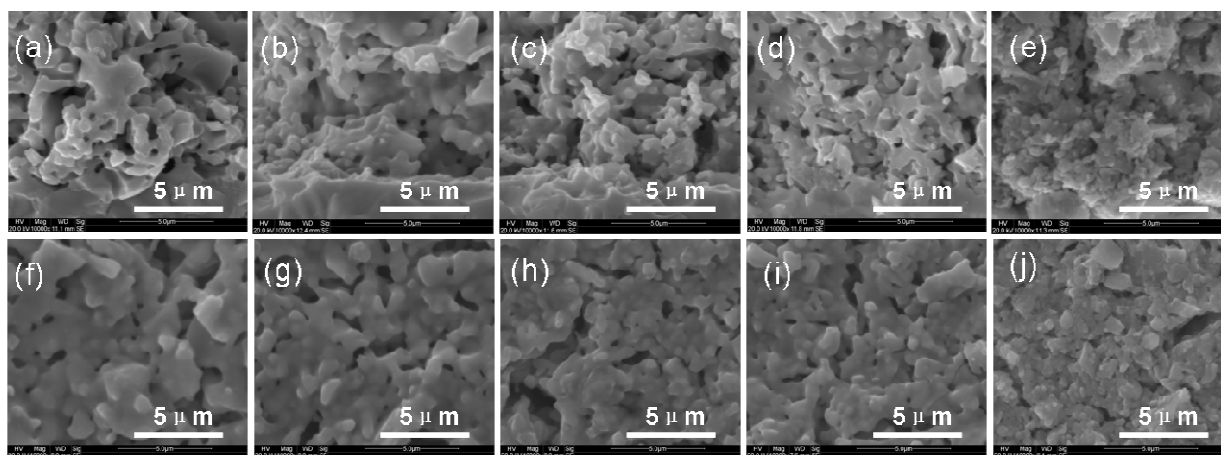
Fig. 4 SEM images of the surface and cross-section of SrNb$_{0.1}$Co$_{0.9-x}$Fe$_x$O$_{3-\delta}$ (0≤x≤0.5) cathodes fired at 1000 °C for 2 h in air: (a, f) x=0, (b, g) x=0.1, (c, h) x=0.2, (d, i) x=0.3, (e, j) x=0.5.

To evaluate the impact of electrode microstructure (e.g. grain size, pore structure and connection with electrolyte) on electrochemical performance, scanning electron microscopy (SEM) images of the surface and cross-section of SNCF cathode after firing at 1000 °C for 2 h are obtained and displayed in **Fig. 4**. Sturdy cathode to electrolyte connection is apparent (more clear on **Fig. S2** – lower magnification); denoting the thermal compatibility of SNCF perovskite against the SDC electrolyte. Smaller grain size for higher Fe content (e.g. Fe content of 0.3 and more) is likely attributable to the reduced sinterability; consistent with the decreased oxygen non-stoichiometry and diffusion trend delineated above.[48] Given that smaller grain size results in increased surface area (at constant volume), reduced sinterability for SNCF may actually be favorable in achieving enhanced ORR activity. Fe doping can therefore be adjusted to manipulate the sinterability of Co-based perovskite cathodes as also reported elsewhere.[38,49] The contribution of the grain size however is not substantial on these SNCF cathodes. It is evident that the ORR activity is closely related to the oxygen non-stoichiometry, as the highest ORR activity of SNCF0.1 and SNCF0.2 (e.g. lowest ASRs) correlates with the largest oxygen non-stoichiometry values of these cathodes. To a minor extent, smaller grain size of SNCF0.2 may contribute to the slightly higher ORR activity for SNCF0.2 at 500 and 550 °C. However, larger grain size of SNFC0.2 (relative to the grain size of SNCF0.3 and SNCF0.5) does not translate to higher ORR activity for SNFC0.3 and SNFC0.5, which rules out dominant grain size influence.

Although it is not likely, the phase transition at high temperature may occur and significantly influence the ORR activity.[40,50-52] The possibility of such transition on the SNCF perovskite was checked by annealing them at high temperature followed by quenching to room temperature (to preserve their high temperature crystalline structure). Powder x-ray diffraction (XRD) patterns of the SNCF0.1-0.5 quenched from 500 and 700 °C are contrasted against their room temperature counterparts in **Fig. 5** which shows no indication of any phase transition for any composition.

We take a highly active cathode, BSCF as a baseline to illustrate factors affecting phase stability of the perovskites. BSCF, particularly at high Ba and Co content e.g. 50% Ba and 80% Co is characterised by a pronounced size mismatch between A- and B-site cations. This attribute facilitates the reduction of B-site cations which leads to an increased effective ionic radius, a higher oxygen deficiency as well as reduction in oxygen vacancy migration barriers. Despite its beneficial effects to ionic conductivity and oxygen exchange kinetics, this A- and B-site cation size mismatch also destabilises the cubic perovskite structure, driving the formation of hexagonal phase exhibiting lower ionic conductivity and slower kinetics.[44,53,54] To solve this structure issue, for example the hexagonal phase formation can be suppressed by adding low amount of high-valence cations such as Nb^{5+} in B-site.[55] The exclusion of large size Ba cation from the A-site minimise the mismatch further. In addition, partial substitution of Co in SNC with Fe is expected to provide improved phase stability considering higher covalency of Fe-O bond compared to Co-O bond.[56]
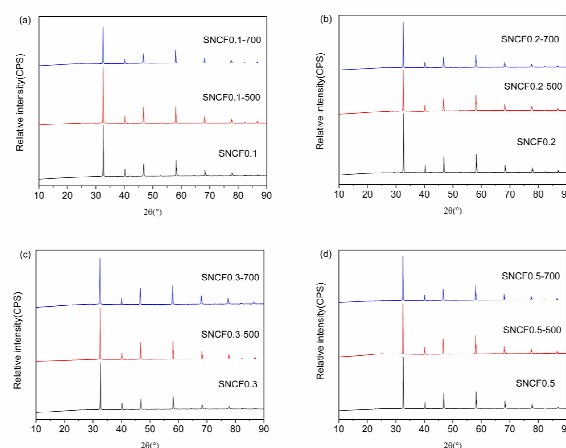

Fig. 5 Powder x-ray diffraction patterns of SNCF (x=0.1-0.5) powders quenched from 500 and 700 °C including as-synthesised ones for comparison. (a) SNCF0.1; (b) SNCF0.2; (c) SNCF0.3; (d) SNCF0.5.

The electrochemical performance of SNFC0.2 was further tested using an SDC-Ni (50:50 vol. %) anode-supported SDC (20 μm) electrolyte single cell. The voltage and power density polarisation curves of a single fuel cell were obtained with
5 hydrogen as a fuel and ambient air as the oxidation agent between 400-600 ^{o}C (**Fig. 6a**). The peak power densities were
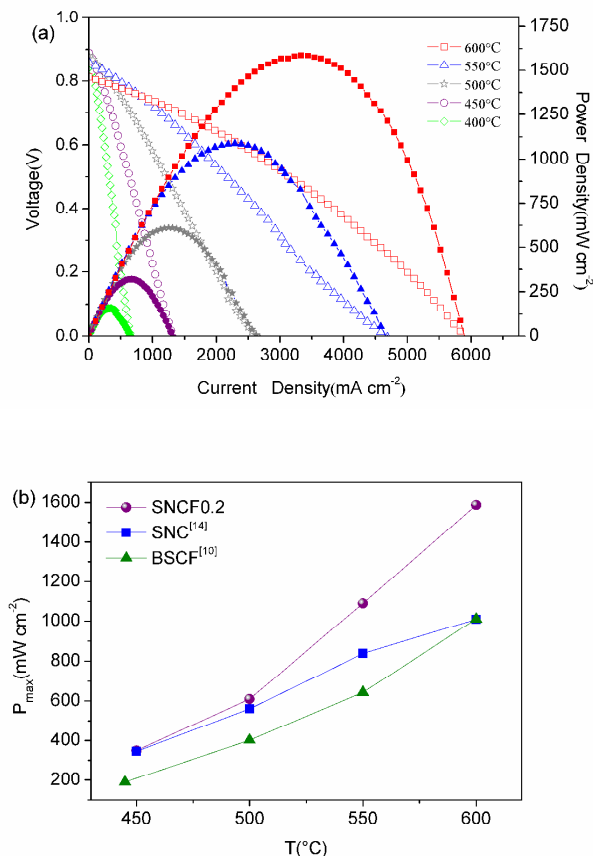

Fig. 6 (a) Voltage and power density polarisation curves of the single
10 fuel cell based on SNCF0.2 cathode between 400-600 ^{o}C; (b) Peak power densities of SNCF0.2, BSCF and SNC cathodes in identical single fuel cell configuration between 450 -600 ^{o}C.

610, 1089 and 1587 mW cm^{-2} at 500, 550 and 600 ^{o}C, respectively; the highest reported to date. **Fig. 6b**, in turn,
15 compares the peak power densities of SNCF0.2 to those of BSCF[10] and the parent compound, SNC[14]; highlighting its superior cell performance. Further performance improvement is an open possibility; offered via an engineering approach such as thickness reduction and microstructure optimisation.
20 Another piece of supporting data obtained by impedance spectroscopy is summarised in **Fig. 7** which plots the resistance of fuel cell components e.g. electrode (cathode plus anode) and electrolyte between 500-600 ^{o}C. The polarisation resistances of the electrode are as low as 0.025 and 0.113 Ω
25 cm^2 at 600 and 500 ^{o}C, respectively. Notably, the resistances of the electrode in the single fuel cell are different from that of the symmetric cell due to the different testing condition imposed e.g. symmetric cell were tested under open circuit voltage while full cell were tested under cathodic polarisation
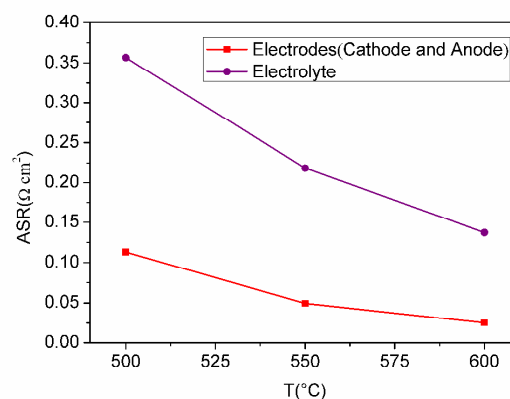30 condition.

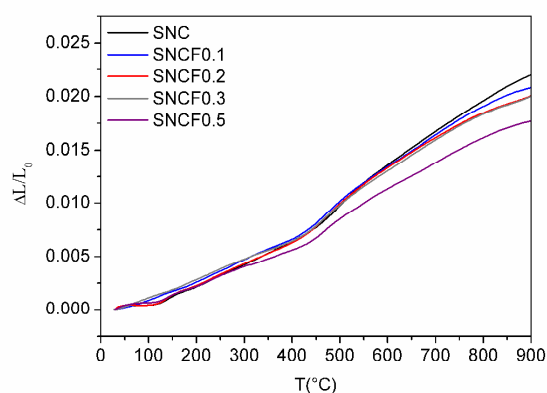**Fig. 7** Electrodes and electrolyte polarisation resistances of single fuel cell between 500-600 ^{o}C.

35

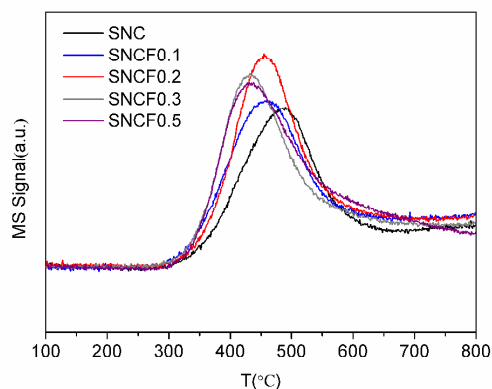**Fig. 8** Thermal expansion curves of SNCF between 25-900 ^{o}C in air.

Fig. 9 O$_2$-temperature programmed desorption profiles of SNCF.

Fig. 8 shows the thermal expansion curve of SNCF
40 (0≤x≤0.5) between 25-900 ^{o}C in air. An inflection in the curve is observed at ~450 ^{o}C which correlates with the reduction of Co^{4+} or Fe^{4+} to Co^{3+} or Fe^{3+} indicated by oxygen-temperature programmed desorption (O$_2$-TPD) results (**Fig. 9**). The average TEC values of SNCF and SDC[57] are listed in **Table 4**;
45 the values of which decreases with increasing Fe content. This

may be due to the stronger Fe-O bond (with respect to the Co-O bond).[58] Low TEC normally leads to better structural stability in long term operation and during thermal cycling.

Table 4 TECs for SNCF samples between RT and 900 °C in air.

Samples	TEC $(\times 10^{-6}\ K^{-1})$		
	RT-450 °C	450-900 °C	RT-900 °C
SNC	19.2	31.5	27.9
SNCF0.1	19.0	28.5	26.4
SNCF0.2	18.7	26.9	26.0
SNCF0.3	18.1	26.7	25.1
SNCF0.5	16.1	24.4	22.3
SDC[59]	12.3 (30-800 °C)		

Resistance to carbon dioxide adds to the practical value of a cathode due the presence of this gas in ambient atmosphere and fuel (as a product of synthesis gas), particularly when the application in single chamber SOFC is envisioned. Alkaline earth containing perovskites are normally prone to CO_2 poisoning.[59-61] To determine its resistance to CO_2, the ASR of SNCF cathodes at 600 °C is monitored before and after introducing CO_2 (in varying concentration between 1-10 vol.% CO_2) into the cathode side (**Fig. 10**). Relative to BSCF and the parent compound, SNC, SNCF cathodes show marginal increase in their ASR values. We attributed the observed stability to the higher acidity of the metal oxide in SNCF perovskites.[62] Furthermore, although all compounds shows the regeneration ability when air was introduced back into the atmosphere, SNFC cathodes can rapidly recover their original ASR values. CO_2 effect on the SNCF0.2 and BSCF was examined by powder x-ray diffraction (**Fig. S3**) and Fourier-Transform Infra-Red spectra (**Fig. S4**). Both results reveal the remarkably improved CO_2-tolerance on the SNCF0.2. While carbonate phases is observed in the powder XRD of CO_2 treated BSCF, they don't exist in SNCF0.2. Accordingly, there is a negligible indication of vibration in the wavelength characteristic of carbonate functional groups for SNCF0.2 which on the other hand is quite substantial in BSCF case.
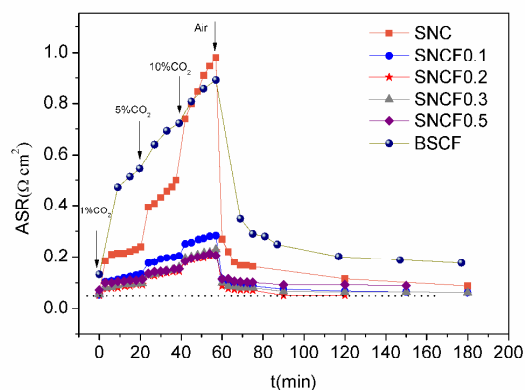

Fig. 10 Stability tests results of SNCF, BSCF and SNC cathodes at 600 °C subjected to air containing varying amount of CO_2.

4. Conclusions

In sum, a new family of $SrNb_{0.1}Co_{0.9-x}Fe_xO_{3-\delta}$ (SNCF, $0.1 \leq x \leq 0.5$) perovskite have been developed which exhibits improved cathode attributes with respect to their parent compound, $SrNb_{0.1}Co_{0.9}O_{3-\delta}$ (SNC). Partial Co substitution with Fe enhanced the ORR activity, reduced the TECs and increased CO_2 resistance. These properties closely correlated with the oxygen non-stoichiometry trend and sinterability behavior. Of all doped compounds, SNFC0.2 demonstrates the highest ORR activity.

Acknowledgements

Notes and references

[a]State Key Laboratory of Materials-Oriented Chemical Engineering
College of Chemistry & Chemical Engineering
Nanjing Tech University
No. 5 Xin Mofan Road, Nanjing 210009 (P.R. China)
[b]Department of Chemistry
University of Waterloo
200 University Avenue West, Waterloo, Ontario, N2L 3G1, (Canada)
[c]School of Chemical Engineering
The University of Queensland
Brisbane, Queensland 4072 (Australia)
E-mail: wei.zhou@uq.edu.au
[d]State Key Laboratory of Materials-Oriented Chemical Engineering
College of Energy
Nanjing Tech University
No. 5 Xin Mofan Road, Nanjing 210009 (P.R. China)
E-mail: shaozp@njtech.edu.cn

† Electronic Supplementary Information (ESI) available: [details of any supplementary information available should be included here]. See DOI:10.1039/b000000x/

5 1   E. D. Wachsman and K. T. Lee, *Science* 2005, **334**, 935.
2   J. M. Vohs and R. J. Gorte, *Adv. Mater.* 2009, **21**, 943.
3   S. M. Haile, *Acta Mater.* 2003, **51**, 5981.
4   W. Zhou, F. L. Liang, Z. P. Shao, J. L. Chen and Z. H. Zhu, *Sci. Rep.* 2011, **1**, 155.
10 5   A. Chroneos, B. Yildiz, A. Tarancon, D. Parfitt and J. A. Kilner, *Energy Environ. Sci.* 2011, **4**, 2774.
6   D. J. L. Brett, A. Atkinson, N. P. Brandon and S. J. Skinner, *Chem. Soc. Rev.* 2008, **37**, 1568.
7   T. Hibino, A. Hasimoto, T. Inoue, J.-I. Tokuno, S.-I. Yoshida and M. Sano, *Science* 2000, **288**, 2031.
15 8   J. Fleig, *J. Power Sources* 2002, **105**, 228.
9   A. J. Jacobson, *Chem. Mater.* 2010, **22**, 660.
10   Z. P. Shao and S. M. Haile, *Nature* 2004, **431**, 170.
11   M. R. Li, W. Zhou, X. Y. Xu and Z. H. Zhu, *J. Mater. Chem. A* 2013,
20   **1**, 13632.
12   S. S. Jiang, J. Sunarso, W. Zhou and Z. P. Shao, *J. Mater. Chem. A* 2013, **1**, 11026.
13   F. L. Liang, W. Zhou, J. Li and Z. H. Zhu, *J. Mater. Chem. A* 2013, **1**, 13746.
25 14   W. Zhou, Z. P. Shao, R. Ran, W. Q. Jin and N. P. Xu, *Chem. Commun.* 2008, 5791.
15   W. Zhou, Z. P. Shao, R. Ran and R. Cai, *Electrochem. Commun.* 2008, **10**, 1647.
16   W. Zhou, F. L. Liang, Z. P. Shao and Z. H. Zhu, *Sci. Rep.* 2012, **2**,
30   327.
17   S.S. Jiang, W. Zhou, F. L. Liang and Z. P. Shao, *J. Mater. Chem.* 2012, **22**, 16214.
18   A. Heel, P. Holtappels and T. Graule, *J. Power Sources* 2010, **195**, 6709.
35 19   M. Yano, A. Tomita, M. Sano and T. Hibino, *Solid State Ionics* 2007, **177**, 3351.
20   I. Riess, *J. Power Sources* 2008, **175**, 325.
21   A. Coelho, 2008, DIFFRACplus TOPAS 4.2, Karlsruhe, Germany, Bruker AXS GmbH.
40 22   R. D. Shannon, *Acta Cryst.* 1976, **A32**, 751.
23   G. L. Miessler and P. J. Fischer, D. A. Tarr, *Inorganic Chemistry*, 5th edtion, Pearson Education Inc., United States, Chapter 10.3. Ligand Field Theory, 2014, 373.
24   W. Zhou, B. M. An, R. Ran and Z. P. Shao, *J. Electrochem. Soc.*
45   2009, **156**, B884.
25   F. F. Dong, D. J. Chen, Y. B. Chen, Q. Zhao and Z. P. Shao, *J. Mater. Chem.* 2012, **22**, 15071.
26   W. Zhou, J. Sunarso, Z.-G. Chen, L. Ge, J. Motuzas, J. Zou, G. X. Wang, A. Julbe and Z. H. Zhu, *Energy Environ. Sci.* 2011, **4**, 872.
50 27   J. H. Kim and A. Manthiram, *J. Electrochem. Soc.* 2008, **155**, B385.
28   .B. C. H. Steele, *Solid State Ionics* 1996, **86-88**, 1223.
29   S. B. Adler, *Solid State Ionics* 1998, **111**, 125.
30   W. Zhou, J. Sunarso, M. W. Zhao, F. L. Liang, T. Klande and A. Feldhoff, *Angew. Chem. Int. Ed.* 2013, **52**, 14036.
55 31   G. Kim, S. Wang, A. J. Jacobson, L. Reimus, P. Brodersen and C. A. Mims, *J. Mater. Chem.* 2007, **17**, 2500.
32   Y. L. Zhu, Z. G. Chen, W. Zhou, S. S. Jiang, J, Zhou and Z. P. Shao, *ChemSusChem* 2013, **6**, 2294.
33   E. Perry Murray, M. J. Sever and S. A. Barnett, *Solid State Ionics*
60   2002, **148**, 27.
34   C. Setevich, F. Prado, D. Z. de Florio and A. Caneiro, *J. Power Sources* 2014, **247**, 264.
35   C. J. Zhu, X. M. Liu, C. S. Yi, L. Pei, D. T. Yan, J. P. Niu, D. J. Wang and W. H. Su, *Electrochem. Commun.* 2009, **11**, 958.
65 36   S. Choi, S. Yoo, J. Kim, S. Park, A. Jun, S. Sengodan, J. Kim, J. Shin, H. Y. Jeong, Y. Choi, G. Kim and M. L. Liu, *Sci. Rep.* 2013, **3**, 2426.
37   J. Kim, A. Jun, J. Shin and G. Kim, *J. Am. Ceram. Soc.* 2014, **97**, 651.
38   Y. N. Kim, J.-H. Kim and A. Manthiram, *J. Power Sources* 2010, **195**, 6411.
70 39   W. Zhou, Z. P. Shao, R. Ran, P. Y. Zeng, H. X. Gu, W. Q. Jin and N. P. Xu, *J. Power Sources* 2007, **168**, 330.

40   S. S. Jiang, W. Zhou, Y. J. Niu, Z. H. Zhu and Z. P. Shao, *ChemSusChem* 2012, **5**, 2023.
41   X. J. Chen, S. H. Chan and K. A. Khor, *Electrochim Acta* 2004, **49**,
75   1851.
42   M. J. Jørgensen and M. Mogensen, *J. Electrochem. Soc.* 2001, **148**, A433.
43   M. J. Escudero, A. Aguadero, J. A. Alonso and L. Daza, *J. Electroanal. Chem.* 2007, **611**, 107.
80 44   M. M. Kuklja, E. A. Kotomin, R. Merkle, Yu. A. Mastrikov and J. Maier, *Phys. Chem. Chem. Phys.* 2013, **15**, 5443.
45   F. S. Baumann, J. Fleig, H. U. Habermier and J. Maier, *Solid State Ionics* 2006, **177**, 3187.
46   Y. J. Niu, J. Sunarso, F. L. Liang, W. Zhou, Z. H. Zhu and Z. P. Shao,
85   *J. Electrochem. Soc.* 2011, **158**, B132.
47   D. J. Chen, F. C. Wang, H. G. Shi, R. Ran and Z. P. Shao, *Electrochim Acta* 2012, **78**, 466.
48   J. W. Stevenson, P. F. Hallman, T. R. Armstrong and L. A. Chick, *J. Am. Ceram. Soc.* 1995, **78**, 507.
90 49   S. Choi, J. Shin and G. Kim, *J. Power Sources* 2012, **201**, 10.
50   W. Zhou, J. Sunarso, J. Motuzas, F. L. Liang, Z. G. Chen, L. Ge, S. M. Liu, A. Julbe and Z. H. Zhu, *Chem. Mater.* 2011, **23**, 1618.
51   M. Arnold, Q. Xu, F. D. Tichelaar and A. Feldhoff, *Chem. Mater.* 2009, **21**, 635.
95 52   M. Arnold, T. M. Gesing, J. Martynczuk and A. Feldhoff, *Chem. Mater.* 2008, **20**, 5851.
53   D. N. Mueller, R. A. De Souza, H. I. Yoo and M. Martin, *Chem. Mater.* 2012, **24**, 269.
54   D. N. Mueller, R. A. De Souza, T. E. Weirich, D. Roehrens, J. Mayer
100   and M. Martin, *Phys. Chem. Chem. Phys.* 2010, **12**, 10320.
55   T. Nagai, W. Ito and T. Sakon, *Solid State Ionics* 2007, **177**, 3433.
56   K. T. Lee and A. Manthiram, *Chem. Mater.* 2006,**18**, 1621.
57   S. Y. Li, Z. Lü, B. Wei, X. Q. Huang, J. P. Miao, Z. G. Liu and W. H. Su, *J Alloys Compd* 2008, **448**, 116.
105 58   K. T. Lee and A. Manthiram, *Solid State Ionics* 2005, **176**, 1521.
59   J. Yi, S. J. Feng, Y. B. Zuo, W. Liu and C. S. Chen, *Chem. Mater.* 2005, **17**, 5856.
60   J. Yi, T. E. Weirich and M. Schroeder, *J. Member. Sci.* 2013, **437**, 49.
61   Q. Zeng, Y. B. Zu, C. G. Fan and C. S. Chen, *J. Member. Sci.* 2009,
110   **335**, 140.
62   J. Yi, M. Schroeder, T. Weirich and J. Mayer, *Chem. Mater.* 2010, **22**, 6246.
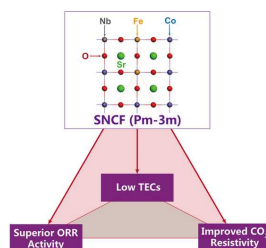
A novel family perovskite $SrNb_{0.1}Co_{0.9-x}Fe_xO_{3-\delta}$ (SNCF, $0.1 \leq x \leq 0.5$) shows not only high oxygen-reduction-reaction activity at operating temperatures below 600 ºC (e.g. peak power density of 1587 mW cm^{-2} at 600 ºC) but also low TECs and improved CO_2 resistivity.